Ab Initio MO Study of the Structures of N_2, NO, and CO Molecules Coordinated to the Pd_n (n = 1, 2, 5, 25) Clusters as a Model of Pd(110) Surface

Toshiaki Matsubara,*,† Tomoko Nagai,† Masataka Nagaoka,*,‡ and Tokio Yamabe†

Institute for Fundamental Chemistry, 34-4 Takano-Nishihiraki-cho, Sakyo-ku, Kyoto 606-8103, Japan, Graduate School of Human Informatics, Nagoya University, Chikusa-ku, Nagoya 464-8601, Japan

Received: October 19, 2000; In Final Form: January 26, 2001

The structures of N_2, NO, and CO molecules coordinated to the Pd_n (n = 1, 2, 5, 25) clusters as a model of Pd(110) surface were investigated by means of ab initio MO methods. All three molecules, N_2, NO, and CO, coordinate to the one Pd atom by the end-on mode, where the tilted end-on structure is more favorable for NO due to the additional electron in the π^* orbital. On the contrary, in the Pd_2 system, N_2 coordinates to the bridge site of Pd_2 cluster preferably by the side-on mode as reported previously (Blomberg et al. *Chem. Phys. Lett.* **1991**, *179*, 524−530), although NO and CO prefer the end-on structure. On the other hand, on the hollow site of the Pd_5 cluster which is the (1 × 1) surface unit of Pd(110) with one Pd atom in the second layer, the tilted structures with an unconventional coordination mode with the interaction of the admolecule with the Pd atoms in both first and second layers were found for all three molecules. With the further extension of the cluster model from the Pd_5 cluster to the Pd_{25} of the (3 × 3) surface unit of Pd(110) including Pd atoms up to the third layer, it was suggested that the nonpolar N_2 and polar CO molecules favorably coordinate to the top and the short-bridge sites, respectively, by the end-on mode in agreement with the experimental finding. Those coordination structures and site preferences are discussed in terms of the electron donation and back-donation between the Pd atoms and N_2, NO, and CO molecules.

1. Introduction

The heterogeneous catalysts have a huge potential in the wide range of industrial reaction processes. For instance, the decomposition of noxious CO, NO_x, and hydrocarbon substrates, included in exhausted gases from the automobile, is one of the great topics in pollution chemistry. The ammonia synthesis from N_2 and H_2 molecules on the surface of iron is industrially the most well-known heterogeneous catalytic reaction in the world. As the adsorption and breaking of N_2 molecule have been considered to be the rate-limiting step in the ammonia synthesis process, the desorption and adsorption of N_2, NO, and CO molecules on the surface of metal are generally thought to be quite important to understand the mechanism of the reaction on the surface of metal. Therefore, the geometric and electronic structures of adsorbed molecules on metal surfaces have been examined for a long time.[1]

On one hand, the coordination of the N_2 molecule to various metals has attracted much attention from many chemists for the last few decades because of the chemical and biological interests and has been extensively studied not only experimentally[2] but also theoretically.[3−5] The coordination modes, end-on and side-on, of the N_2 molecule (Figure 1) are subjects of general interest as those of H_2 molecule have been actively examined so far.[6]

By the ab initio molecular orbital (MO) method, Sakaki et al. have shown that N_2 coordinates to the unsaturated mononuclear complex, $RhCl(PH_3)_2$, by the end-on mode.[3] In contrast to this, in the dinuclear Pd_2 cluster, N_2 coordinates to the bridge site favorably by the side-on mode as demonstrated by Blomberg et al.[4] On metal surfaces, the coordination of N_2 by both end-on and side-on modes has been experimentally observed by some spectroscopic techniques.[7−9] For example, on Fe(111) surface, it was revealed by the photoelectron and high-resolution electron energy-loss spectroscopy (HREELS) that the transformation between the two states of the equilibrium structures of N_2, γ (end-on) and α (side-on) states, takes place. The N−N bond of the side-on bonded structure is broken to form the atomic N-bonded structure (β state).[8] However, despite the tremendous accumulation of results based on the spectroscopic analyses,[10] the microscopic features of geometric and electronic structures of the adsorbed N_2 molecule are still at issue, although the coordination mode has been qualitatively known.

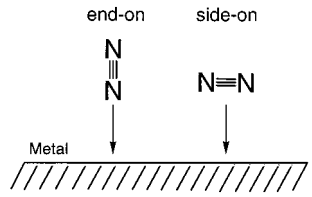

Figure 1. End-on and side-on modes for the coordination of N_2 molecule.

On Pd(110) surface, the coordination structures depending on the admolecules have been considered. The chemisorption of N_2 to the top site with the upright-linear structure has been experimentally suggested by the vibrational electron energy loss spectroscopy (EELS), low-energy electron diffraction (LEED), and Auger electron spectroscopy (AES).[9] On the other hand, the coordination of CO to the short-bridge site with the tilted structure was shown by computations with the density functional theory.[11−13] Thus, the character of the admolecules and the metal might be an essential factor for the coordination structure.

In the present study, we focused on the coordination mode of N_2, NO, and CO molecules on palladium and investigated

† Institute for Fundamental Chemistry.
‡ Nagoya University.

10.1021/jp0038613 CCC: $20.00
Published on Web 04/03/2001

TABLE 1: Basis Sets I−VI

basis set	Pd	C, N, O
I	(5s,4p,4d)/[3s,3p,2d]+ ECP	lanl2dz
II	(5s,4p,4d)/[3s,3p,2d]+ ECP	6-31G(d)
III	(5s,4p,4d,1f)/[3s,3p,3d,1f] + ECP	6-31G(d)
IV	(5s,4p,4d,1f)/[3s,3p,3d,1f] + ECP	6-31+G(d)
V	(5s,4p,4d,1f)/[3s,3p,3d,1f] + ECP	6-311+G(d)
VI	(3s,3p,4d)/[1s,1p,1d] + ECP	6-31G(d)

by means of ab initio MO methods the structures of the coordinated N_2, NO, and CO to the various Pd clusters, Pd_n ($n = 1, 2, 5, 25$), as a model of Pd(110) surface. As a Pd_5 cluster, the 2Pd-layered (1×1) surface unit of Pd(110) was used and was extended to the Pd_{25} cluster to model Pd(110) surface which includes the Pd atoms up to the third layer. Following the explanation of the Computational Details in section 2, we will discuss in section 3 at first the coordination structures of N_2, NO, and CO in the small Pd cluster systems of Pd_1 (section 3.1), Pd_2 (section 3.2), Pd_5 (section 3.3). In section 3.4, the site preference of nonpolar N_2 and polar CO molecules for the large cluster system of Pd_{25} is discussed. Conclusions are summarized in the final section.

2. Computational Details. *2.1. Calculation Methods.* All calculations of geometry optimizations and energetics were performed using Gaussian98 program.[14] The geometry optimizations for the small cluster systems, Pd_n ($n = 1, 2, 5$), were carried out with the two kinds of basis sets, I and III, at the B3LYP level of density functional theory, which consists of a hybrid Becke + Hartree−Fock exchange and Lee−Yang−Parr correlation functional with nonlocal corrections.[15] The basis set I consists of the lanl2dz for C, N and O, and a valence double ζ (5s,5p,4d)/[3s,3p,2d] basis function and the relativistic effective core potential (ECP) replacing the core electrons up to 3d determined by Hay and Wadt[16] for Pd (Table 1).

In the set III, the basis functions which include the polarization function, 6-31G(d)[17] for C, N and O, and the triple ζ (5s,5p,4d)/[3s,3p,3d] augmented by an additional single set of f orbitals with exponent of 1.472 for Pd[18] were used. We will refer only to the results obtained with the higher quality basis set III in the following discussion unless otherwise indicated. However, the results for the geometries and energies obtained with the basis set I were qualitatively similar to those obtained with the basis set III except for only a few cases as shown in the Figures and Tables.

The energy calculations for the Pd_5-N_2 system were also carried out by the second and fourth-order Møller−Plesset perturbation (MPm; $m = 2, 4$) theory and the quadratic configuration interaction method with single and double substitutions (QCISD) in addition to the B3LYP level of theory using the various basis sets II−V as summarized in Table 1 to confirm that the sequence of the stability of the N_2-coordinated structures obtained at the B3LYP level does not change at the other level of theory. For N, 6-31G(d) in the set II was used, and the larger basis sets, 6-31+G(d) in the set IV and 6-311+G(d) in the set V, were used. For Pd, the basis functions used in the sets I and III were also used in the sets II and in IV and V, respectively. Here, we used the optimized structures at the B3LYP/I level for those energy calculations. In fact, the energies calculated at the B3LYP/III//B3LYP/I level showed the excellent agreement with those calculated at the B3LYP/III//B3LYP/III level for the Pd_5-N_2 system as shown in Table 2. Therefore, we also determined the potential energy surface of the transformation between the two equilibrium structures, **3NNa** and **3NNb**, at the B3LYP/I level. The thermochemical parameters, enthalpy, entropy, and Gibbs free energy, were also calculated at the B3LYP/I level for the Pd_5-N_2 system with a scale factor of 0.9614[19] for calculated vibrational frequencies at the temperature of 298.15 K.

The geometry optimizations for the large system, Pd_{25}, were carried out at the Hartree−Fock (HF) level using the basis set VI, that is, 6-31G(d) for N and a (3s,3p,4d)/[1s,1p,1d] basis function and the relativistic ECP replacing the core electrons except the 10 electrons in the valence shell determined by Hay and Wadt[20] for Pd, which well reproduced the tilted structures of N_2 and CO on the Pd_5 cluster optimized at the B3LYP/III level. The energies were recalculated at the B3LYP level with the same basis set VI. In all cases, the calculated energies relative to the free N_2, NO, and CO molecules and Pd_n ($n = 1, 2, 5, 25$) cluster fragments are presented.

2.2. Pd Clusters as a Model of Pd(110) Surface. The bond distances between Pd atoms aligned in the [001] and [1$\bar{1}$0] directions on Pd(110) surface were fixed at 3.767 and 2.650 Å, respectively, which were determined by the optimization for the Pd_{13} cluster, the 2Pd-layered (2×2) surface unit of Pd(110), with the C_{2v} symmetry at the B3LYP/I level within the 4% error compared with the experimental values (3.890 and 2.751 Å, respectively).[21] The distance between the first and second Pd atomic layers was fixed at the experimental value of 1.375 Å.[21]

In the Pd_2 system, we used the two kinds of Pd clusters. One has the short Pd−Pd distance of 2.650 Å and another has the long Pd−Pd distance of 3.767 Å, which correspond to the two

TABLE 2: Calculated Potential Energy (ΔE), Entropy (ΔS), Enthalpy (ΔH), and Gibbs Free Energy (ΔG) at the Various Levels for 3NNa, 3NNb, 3NNc, and 3NNts1 Relative to the Pd_5 Cluster Fragment and Free N_2[a]

	method	Pd_5+N_2(free)[c]	**3NNa**	**3NNb**	**3NNc**	**3NNts1**
ΔE	B3LYP/I	−743.149633	−46.3	−40.2	−39.7	−41.2
	B3LYP/II	−743.187400	−33.5	−29.0	−28.7	−29.6
	B3LYP/III[b]	−743.192173	−36.1	−29.9	−29.4	−30.3
		(−743.194270)	(−36.0)	(−30.2)	(−29.7)	(−30.2)
	B3LYP/IV	−743.198454	−33.7	−27.4	−26.8	−27.6
	B3LYP/V	−743.229560	−31.7	−25.0	−24.5	−26.0
	MP2/II	−739.152863	−81.6	−73.2	−69.6	−62.6
	MP4SDQ/II	−739.155719	−65.6	−57.5	−55.6	−54.7
	QCISD/II	−739.179948	−43.2	−39.9	−22.6	−16.2
	MP2/III	−740.621295	−104.4	−93.6	−88.7	−80.6
	MP4SDQ/III	−740.523498	−68.6	−59.1	−56.9	−57.4
	QCISD/III	−740.550207	−41.3	−35.7	−34.1	−30.8
$T = 298.15$ K						
ΔH	B3LYP/I	−743.133633	−43.3	−37.6	−37.2	−39.0
$T\Delta S$	B3LYP/I	0.063355	−7.4	−6.8	−6.5	−7.0
ΔG[d]	B3LYP/I	−743.196989	−36.0	−30.8	−30.8	−32.0

[a] Unit in kcal/mol. [b] The energies in parentheses are calculated at the optimized structures at the B3LYP/III level. [c] Unit in hartrees. [d] The Gibbs free energy is expressed by the equation, $\Delta G = \Delta H - T\Delta S$.

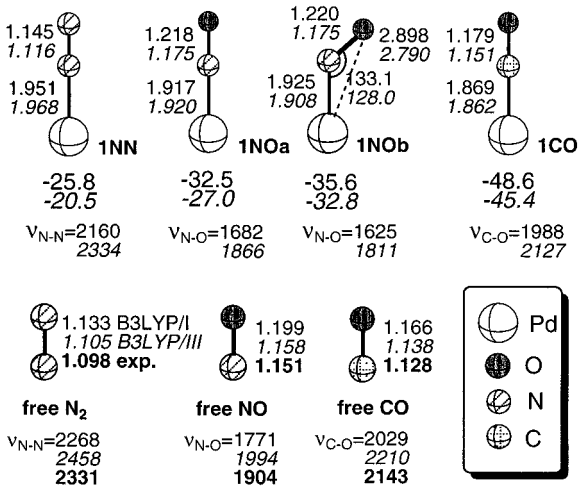

Figure 2. Optimized equilibrium structures of N_2, NO, and CO molecules coordinated to the one Pd atom and the free N_2, NO, and CO molecules with the selected parameters (in Å and degrees) at the B3LYP/I (plain) and B3LYP/III (italics) levels, their energies (in kcal/mol) relative to the one Pd atom and the free N_2, NO, and CO, and the experimentally observed and calculated stretching vibrational frequencies (in cm^{-1}) of N−N, N−O, and C−O bonds at those levels.

Pd atoms aligned in the [1$\bar{1}$0] and [001] directions on Pd(110) surface, respectively. As the Pd_5 cluster, the 2Pd-layered (1 × 1) surface unit of Pd(110) was used and extended to the Pd_{25} cluster to model Pd(110) surface which consists of 12 Pd atoms of the (3 × 3) surface unit of Pd(110) in the first layer, nine Pd atoms in the second layer, and four Pd atoms in the third layer as presented in Figures 8 and 9. In optimizations, all of the Pd atoms were frozen with the lattice parameters mentioned above. No symmetry was found unless otherwise indicated except for the Pd_{25} system. In the optimizations for Pd_{25} system, we forced the N_2 and CO molecules to keep the true end-on or side-on configuration except the tilted structures on the hollow site. We used the labels, **1**, **2**, **3**, and **4**, for the Pd_1, Pd_2, Pd_5, and Pd_{25} systems, and **NN**, **NO**, and **CO** for the N_2, NO, and CO molecules, respectively. In the Pd_2 system, the end-on and side-on bonded structures are labeled by **E** and **S**, respectively, and **l** and **s** denote the long and short Pd_2 clusters, respectively.

3. Results and Discussion

3.1. Pd_1 System. We at first examined the coordination structures of N_2, NO, and CO on the one Pd atom, which is the most simple coordination site model for Pd(110) surface. For all three molecules, only the end-on bonded structures were found, as presented in Figure 2.

N_2. For N_2, the Pd−N−N axis is linear and the N−N bond distance is stretched by 0.011 Å compared with that of free N_2. The calculated vibrational frequency of 2334 cm^{-1} for the N−N bond is consistently smaller than that of 2458 cm^{-1} for the free N_2.[22] Another N_2 coordination by the side-on mode was not found. The optimized side-on bonded N_2 with the C_{2v} symmetry constraint was less stable by 8.6 kcal/mol than **1NN**. When the symmetry restriction is released, the end-on bonded structure, **1NN**, was obtained by the geometry optimization. The similar end-on coordination preference has been reported for the phosphine-coordinated mononuclear Rh complex system.[3] The interaction of N_2 with the metal atom is generally well expressed by the two kinds of charge transfers, that is, the electron donation from the pσ orbital of N_2 to the unoccupied dσ orbital of the metal atom and the electron π-back-donation from the occupied dπ orbital of the metal atom to the pπ^* orbital of N_2 illustrated below.

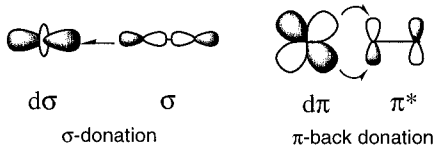

In the present case, the electron π-back-donation is considered to be dominant, because the metal is the d^{10} Pd atom. The orbital overlap in the π-back-donation interaction might be smaller in the side-on bonded geometry than in the end-on bonded one by the geometrical reason. The Mulliken bond population between Pd and N_2 in the artificial side-on bonded structure with the C_{2v} symmetry was about half of that in the end-on bonded structure, **1NN**, supporting this assumption.

NO. Two equilibrium structures were found on the NO coordination by the end-on mode. One is **1NOa** with the Pd−N−O axis being completely linear. Another structure **1NOb** has the Pd−N−O axis with the angle of 128.0°, which is obviously different from **1NOa**. The similar coordination feature of NO with a tilt angle has also been reported for the mononulcear Co complex system.[23] Since NO has the additional one electron in the pπ^* orbital, the electron donation from the pπ^* orbital of NO to the dσ+sp hybridized orbital of Pd in addition to the back-donation from the occupied dπ orbital of Pd to the unoccupied pπ^* orbital of NO occurs, which results in the bend of the Pd−N−O axis for the better overlap between those orbitals as presented below.

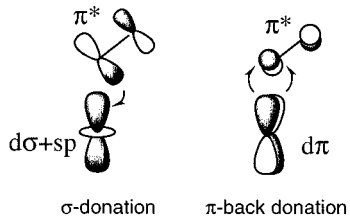

By this interaction, **1NOb** is 5.8 kcal/mol more stable than **1NOa**. The repulsive interaction between the negatively charged oxygen of NO and the electron-rich Pd atom does not allow NO to coordinate by the side-on mode to the Pd atom.

CO. Another polar molecule, CO, also did not give the side-on bonded structure. The coordination of CO by the end-on mode shows the linear Pd−C−O axis. The C−O bond distance is stretched by 0.013 Å compared with that of the free CO due to the back-donation from the occupied dπ orbitals of Pd atom to the unoccupied pπ^* orbitals of CO. On comparison among N_2, NO, and CO, the coordination energy of CO, 45.4 kcal/mol, was the largest, the sequence being CO > NO > N_2. This sequence would be rationally understood with the strength of the π-back-donation. It is easily expected that the π-back-donation would be the largest for CO, which is a strong π-acceptor.[24] In fact, the electron population of the dπ orbital of Pd, which is the electron donor in the π-back-donation, showed the order, CO (1.860 e) < NO (1.881 e) < N_2 (1.943 e), indicating the strength of the π-back-donation with the opposite order.

3.2. Pd_2 System. We next examined the coordination of N_2, NO, and CO to the bridge site of Pd_2 cluster. Here, we used the two kinds of the Pd_2 clusters, of which Pd−Pd distances are fixed at the long and short Pd−Pd distances of 3.767 Å and 2.650 Å of the optimized Pd(110) surface unit (see section 2.2).

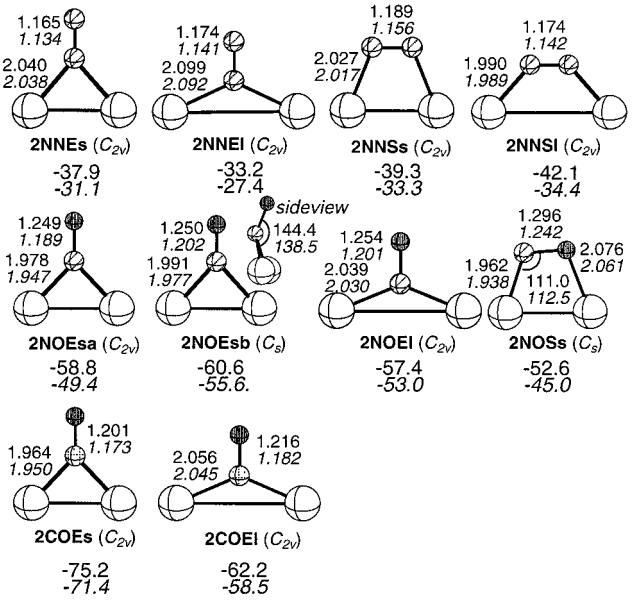

Figure 3. Optimized equilibrium structures of N_2, NO, and CO molecules coordinated to the bridge site of the two kinds of Pd_2 clusters which have short and long Pd−Pd distances (see Computational Details for details) with the selected parameters (in Å and degrees) at the B3LYP/I (plain) and B3LYP/III (italics) levels, and their energies (in kcal/mol) relative to the Pd_2 cluster fragments and the free N_2, NO, and CO at those levels.

N_2. As presented in Figure 3, both end-on and side-on bonded N_2 were found on each short and long Pd_2 cluster model. The distance of Pd−N bond is longer by 0.054 Å in **2NNEl** than in **2NNEs**, while shorter by 0.028 Å in **2NNSl** than in **2NNSs**. Compared with the end-on bonded structures, the side-on bonded ones give the shorter Pd−N bond distances on both short and long bridge compounds, indicating that the Pd−N bonds in the side-on bonded structures are stronger. Thus, on both long and short Pd_2 clusters, the side-on bonded structures were more stable than the end-on bonded ones, which coincides with the result reported by Blomberg et al.[4] although the calculation methods used are different each other. The strength of the interaction by the electron back-donation from the occupied d orbitals of Pd atoms to the unoccupied pπ* orbital of N_2 molecule would be strongly reflected on the sequence of the stability, side-on > end-on. The MO analysis showed that the MO 1 in the end-on bonded structures presented below was somewhat higher in energy than the MO 2 in the side-on bonded structures. The bond populations of Pd−N were also consistently

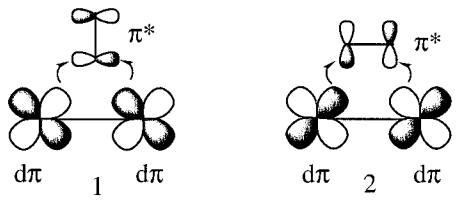

larger by 0.031−0.055 e in the side-on bonded structures than in the end-on bonded structures.

NO. For NO, in addition to the end-on bonded structures with the C_{2v} symmetry, **2NOEsa** and **2NOEl**, the tilted end-on structure, **2NOEsb**, with the C_s symmetry with the tilt angle of 138.5°, was found, which is similar to the case of the Pd_1 system (section 3.1). As shown in the relative energy, **2NOEsb** obtains the larger stabilization by the electron donation from the pπ* orbital of NO to the dσ+sp orbitals of Pd atoms compared with **2NOEsa** and **2NOEl**. Although the interaction between the oxygen and Pd atom is repulsive as mentioned above, the pseudo-side-on structure, **2NOSs**, was also found, due to the electron donation from the pπ* orbital of NO to the dσ+sp orbitals of Pd atoms as presented below. However, the structure,

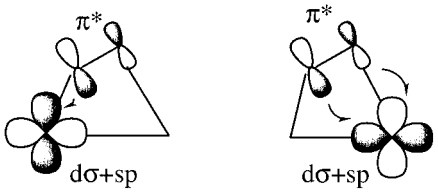

2NOSs, is less stable by 4.4 kcal/mol than the end-on bonded structure, **2NOEsa**, which suggests that the stabilization obtained by the π-back-donation from the dπ orbital of Pd to the pπ* orbital of NO is more important.

CO. On the other hand, the CO molecule without an electron in the pπ* orbital coordinates to the bridge site of Pd_2 cluster by only the end-on mode. The strong π-acceptor CO would induce the strong electron back-donation from the dπ orbitals of Pd to the pπ* orbitals of CO. As well as the Pd_1 system, the Pd_2 system showed the sequence in the coordination energy, CO > NO > N_2, the coordination energy being larger in the Pd_2 system than in the Pd_1 system for all three molecules, N_2, NO, and CO. The coordination energy, which is 12.9 kcal/mol larger for **2COEs** than for **2COEl**, shows that the CO molecule obviously prefers the short-bridge site to get the better orbital overlap with the two Pd atoms.

3.3. Pd_5 System. On Pd(110) surface, the Pd atoms in the second layer as well as the Pd atoms in the first layer are relatively exposed to interact with incoming small molecules because the distance between Pd atoms in the first layer aligned in the [001] direction is much longer than that in the other surfaces such as Pd(100) and Pd(111), which suggests the importance of the hollow site. We therefore investigated the coordination of N_2, NO, and CO molecules to the hollow site of the Pd_5 cluster, the 2Pd-layered (1 × 1) surface unit of Pd-(110).

N_2. As presented in Figure 4, three equilibrium structures of N_2, **3NNa** with the N_2-axis oriented in the [001] direction, and **3NNb** and **3NNc** with the N_2-axis oriented in the [1$\bar{1}$0] direction, were obtained.

In the structure **3NNa**, the N_2-axis makes the tilt angle of 28.8° to the Pd surface and the structure of N_2 is significantly deformed upon comparison to both canonical side-on and end-on bonded structures. The N−N bond distance, 1.210 Å, is longer by 0.105 Å than that of free N_2. The N^1−Pd^5 distance (2.074 Å) is as short as the N^1−$Pd^{3,4}$ distances (2.145 Å), indicating that the N^1 atom interacts with the Pd atom in the second layer as well as those in the first layer. The N^2−$Pd^{1,2}$ bonds also have a short distance of 1.994 Å, while the N^2−Pd^5 distance of 2.622 Å is long. Even if the optimizations were performed with the initial geometries of the true end-on or side-on bonded N_2, **3NNa** was finally obtained. On the basis of the fact that N_2 coordinates to the $Pd^{3,4}$ atoms in the first layer by the end-on mode and simultaneously to both Pd^5 atom in the second layer and $Pd^{1,2}$ atoms in the first layer by the side-on mode, the coordination feature is considered to be a hybrid mode of end-on and side-on. The optimized structure with the C_{2v} symmetry constraint, **3NNts1**, corresponds to the transition state between **3NNa** and **3NNa′** (see Figure 6)**.**

In the structure, **3NNb**, the tilt angle made by the N_2-axis and the Pd surface is reduced to 14.8° although the geometrical

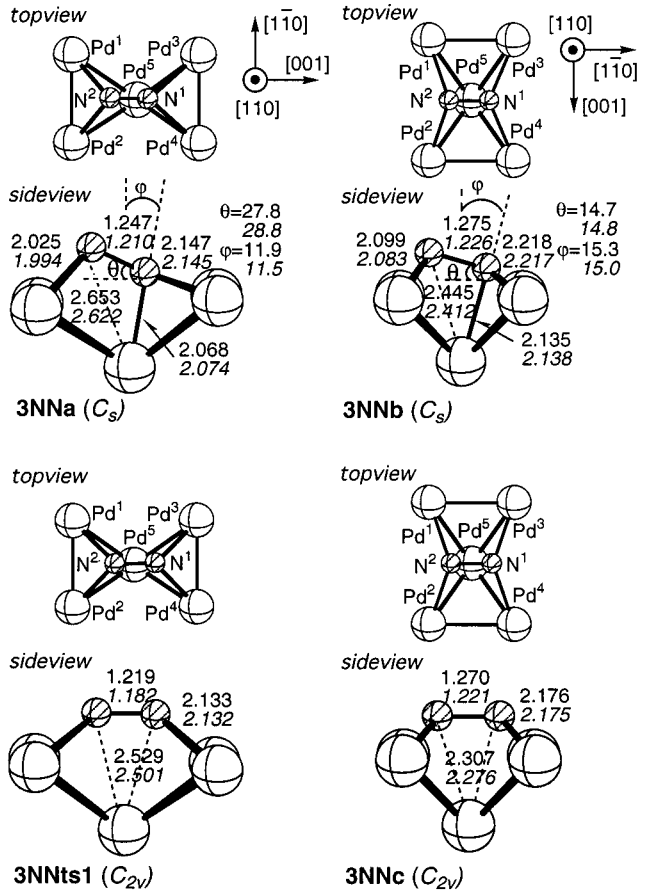

Figure 4. Optimized equilibrium structures of N_2 molecule coordinated to the hollow site of Pd_5 cluster, the 2Pd-layered (1×1) surface unit of Pd(110), with the selected parameters (in Å and degrees) at the B3LYP/I (plain) and B3LYP/III (italics) levels. The angles θ made by the N_2-axis and the Pd surface and φ made by the Pd^5-N^1 and [110] axes are presented. The structure, **3NNts1**, which corresponds to the transition state between **3NNa** and **3NNa′** (see Figure 5), was optimized, imposing the C_{2v} symmetry.

feature of **3NNb** is similar to that of **3NNa**. The distances of N^1-Pd,[5] $N^1-Pd^{3,4}$, and $N^2-Pd^{1,2}$ are longer by 0.054−0.089 Å than those in **3NNa**, which indicates that the interaction of N_2 with the Pd atoms is weaker in **3NNb** than in **3NNa**. On the other hand, in another structure **3NNc** with N_2 oriented in the [1$\bar{1}$0] direction, N_2 coordinates in the conventional side-on fashion so that the N_2-axis is parallel to the Pd surface. The distance of N−Pd,[5] 2.276 Å, is much longer than that of N^1-Pd^5 in **3NNa** and **3NNb**, indicating that the interaction of the N atoms with the Pd atom in the second layer is weaker in **3NNc** than in **3NNa** and **3NNb**.

The energies of **3NNa**, **3NNb** and **3NNc** relative to the Pd_5 cluster fragment and the free N_2 are presented in Table 2. **3NNa** is the most stable in energy with the stability sequence, **3NNa** > **3NNb** > **3NNc** at the B3LYP/I level. This tendency does not change at the B3LYP/II and B3LYP/III levels although the binding energies of N_2 become 10 kcal/mol smaller. The side-on bonded N_2 with the [001] orientation optimized with the C_{2v} symmetry constraint, **3NNts1**, was 5.1 kcal/mol less stable than **3NNa** at the B3LYP/I level, which would be ascribed to the loss of the interaction between N^1 and Pd^5 atom in the second layer. On the other hand, the side-on bonded N_2 with the [1$\bar{1}$0] orientation, **3NNc**, is only 0.5 kcal/mol less stable than **3NNb**, suggesting that the interaction between N^1 and Pd^5 atom in the second layer is weaker in **3NNb** where N_2 is oriented in the [1$\bar{1}$0] direction than in **3NNa** where N_2 is oriented in the [001] direction.

The optimizations with the polarization functions for N and Pd atoms gave the only small changes in the geometrical parameters, which demonstrates that the inclusion of the polarization function is not important in the optimizations for N_2. We therefore calculated the energy at the other level of theory using the structures optimized at the B3LYP/I level, which were also used for the MO analysis at the B3LYP/I level. The potential energy surface of the transformation between **3NNa** and **3NNb** was also obtained at the B3LYP/I level. In the B3LYP energy calculations, the higher quality basis sets II−V including defuse or polarization functions did not make any drastic change in the stability sequence, **3NNa** > **3NNb** > **3NNc**. However, as one can find in Table 2, the polarization function for N is important for the coordination energy in all structures. Therefore, the energies for **3NNa**, **3NNb**, **3NNc**, and **3NNts1** were calculated at the higher level of theory, MPm ($m = 2, 4$) and QCISD, with the basis sets II and III with the polarization function for N. The MP2 calculations overestimate the coordination energy by 21.4−58.1 kcal/mol for the four structures compared with the B3LYP/I calculations. This overestimation was improved by the MP4SDQ and QCISD calculations. In all calculation methods, the same stability sequence, **3NNa** > **3NNb** > **3NNc**, was obtained, showing that the characteristic of the coordination is not dependent on the calculation methods. The fact that **3NNts1** is less stable than the other three structures at the MPm ($m = 2, 4$) and QCISD levels with the basis sets II and III except only the MP4SDQ/III level supports that the interaction between the lower N atom and the Pd atom in the second layer is strong. The tendency in the stability, **3NNa** > **3NNb** > **3NNc**, also did not change in the Gibbs free energy at 298.15 K calculated at the B3LYP/I level, although the Gibbs free energy is smaller by about 10 kcal/mol than the potential energy by the entropy effect and the correction of the thermal energy (including the zero-point energy) on the enthalpy.

The Gibbs free energy surface at 298.15 K for the N_2-coordinated structures calculated at B3LYP/I level are presented in Figure 5. These structures are divided to the two groups by the N_2 molecular orientation, N_2 being oriented in the [001] direction on the left-hand side and in the [1$\bar{1}$0] direction on the right-hand side. The orientation of N_2 can be switched by the two ways of the rotation of N_2 on the Pd surface connecting these two groups on the energy surface. One is the rotation with the variable α, and another is the rotation around the axis parallel to the Pd surface through **3NNts2**. The transformation between **3NNb** and **3NNb′** passing through **3NNc** would be more facile than the transformation between **3NNa** and **3NNa′** passing through **3NNts1**. To switch the orientation of N_2 from [001] to [1$\bar{1}$0] with the variable α, the energy barrier of 15.5 kcal/mol is required. Another path through the transition state, **3NNts2**, in which N_2 is bonded to the hollow site by the end-on mode, has much higher energy barrier of 32.2 kcal/mol, because the cleavage of both bonds between the N^2 and Pd atoms in the first layer and between the N^1 and Pd atom in the second layer is needed for this transformation.

To clarify the nature of the interaction of the N_2 molecule with the Pd atoms of the Pd_5 cluster, the 2Pd-layered (1×1) surface unit of Pd(110), which shows the [001]-selective orientation of the coordinated N_2 molecule, we analyzed the MOs for **3NNa** and **3NNb**. The MO energy diagrams of the formed MOs by the interaction between the N_2 and Pd atoms

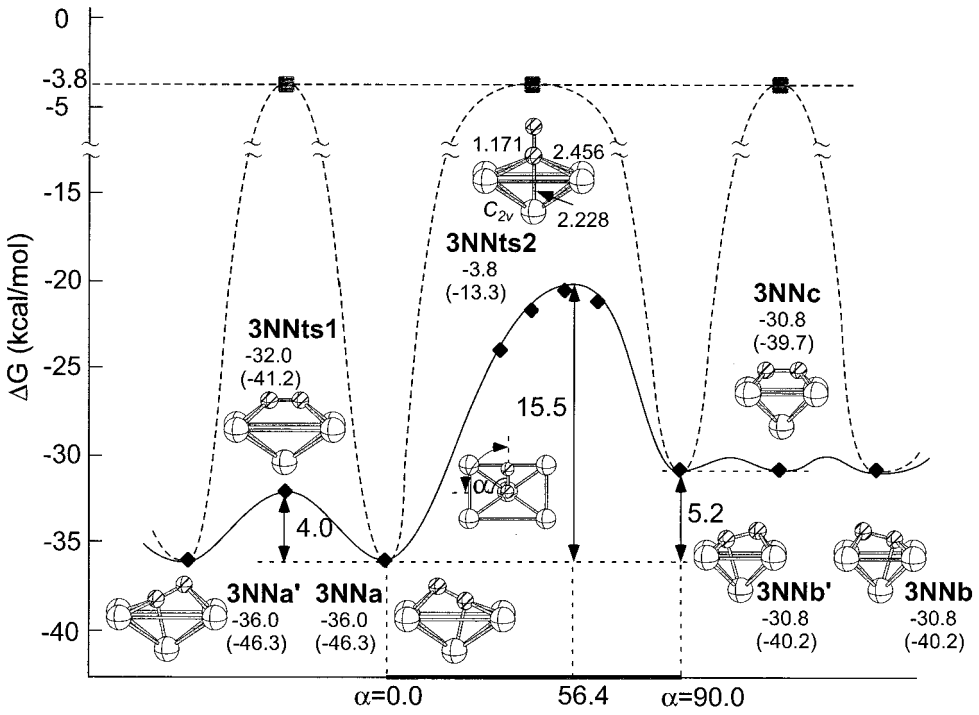

Figure 5. Gibbs free energy surface (in kcal/mol) at 298.15 K calculated at the B3LYP/I level for the structures of N_2 on the hollow site of the Pd_5 cluster, the 2Pd-layered (1×1) surface unit of Pd(110). The solid line shows the transformations between **3NNa** and **3NNa′** through the transition state **3NNts1**, between **3NNb** and **3NNb′** through **3NNc**, and between **3NNa** and **3NNb** with the variable α. The broken line shows those transformations through the transition state **3NNts2**. The numbers in the parentheses are the potential energies calculated at the B3LYP/I level. The optimized parameters (in Å) at the B3LYP/I level are presented for **3NNts2**.

in the first and second layers for **3NNa** and **3NNb** are presented together with the localized MOs in Figure 6.

The interaction of N_2 with the d^{10} Pd atom can be interpreted mainly by the electron back-donation from the occupied d orbitals of Pd to the unoccupied $p\pi^*$ orbitals of N_2. Here, two $p\pi^*$ orbitals of N_2 are distinguished with respect to the orientation of the orbitals. One is perpendicular and another is parallel to the Pd surface, the former and the latter being denoted as $p_\perp$ and $p_{||}$, respectively. In both **3NNa** and **3NNb**, the diagram consists of the five bonding and five corresponding antibonding MOs.[25] The $p_\perp$ orbital of N_2 interacts with the d orbitals of Pd^5 and $Pd^{1,2}$ atoms, while the $p_{||}$ orbital of N_2 interacts with the d orbitals of $Pd^{1,2}$ and $Pd^{3,4}$ atoms through the back-donation. It should be noted here that the former interaction takes place through the σ-back-donation. In **3NNa**, the bonding MO, 28a′, produced by the mixing of the $p_\perp$ orbital of N^1 and the d orbital of Pd,[5] is the lowest in energy among the five bonding MOs. This strong interaction between N^1 and Pd^5 by the σ-back-donation would make the N_2-axis deviate largely from the parallel to the Pd(110) surface (the tilt angle θ is 28.8°, see Figure 4) to get a stabilization.

In **3NNb**, the energy level of the bonding MOs, 30a′ and 40a", where the $p_\perp$ and $p_{||}$ orbitals of N^2 and the d orbitals of $Pd^{1,2}$ in the first layer contribute is lower than that of the corresponding orbitals in **3NNa**. In contrast, the energy level of the bonding MOs, 44a″ and 52a″, where the $p_{||}$ orbital of N^1 and the d orbitals of $Pd^{3,4}$ in the first layer contribute is higher than that of the corresponding orbitals in **3NNa** to countervail the stabilization obtained by the interaction of the N^2 with the Pd.[1,2] The MO, 49a′, where the $p_\perp$ orbital of N^1 and the d orbital of Pd^5 in the second layer dominantly contribute, is not the lowest and much higher in energy than the corresponding MO, 28a′ in **3NNa**. This obviously causes the stability sequence, **3NNa** > **3NNb**. In **3NNb**, the d orbital of Pd,[5] which interacts with the $p_\perp$ orbital of N^1, somewhat inclines as shown by the Pd^5-N^1 axis deviating by 15.0° (11.5° in **3NNa**) from the [110] axis to overlap with the $p_\perp$ orbital of N^1 as much as possible,

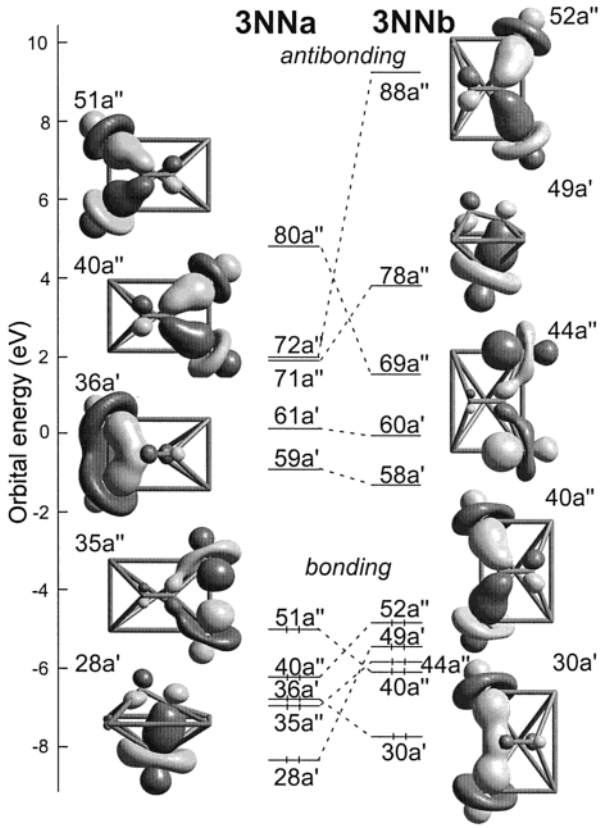

Figure 6. The molecular orbital energy diagrams (in eV) at the B3LYP/I level and the localized molecular orbitals for **3NNa** and **3NNb**. The corresponding molecular orbitals between **3NNa** and **3NNb** are connected each other with the broken line.

TABLE 3: Mulliken Atomic Charges on the N and Pd Atoms in the Structures, 3NNa, 3NNb, and 3NNc Calculated at the B3LYP/I (plain) and B3LYP/III (italics) Levels[a]

	3NNa	3NNb	3NNc	N_2(free)	Pd_5
Pd^1	0.01(−0.03)	0.03(−0.01)	0.07(0.03)		0.04
	0.07(0.02)	*0.07(0.02)*	*0.09(0.04)*		*0.05*
Pd^2	0.01(−0.03)	0.03(−0.01)	0.07(0.03)		0.04
	0.07(0.02)	*0.07(0.02)*	*0.09(0.04)*		*0.05*
Pd^3	0.16(0.12)	0.13(0.09)	0.07(0.03)		0.04
	0.14(0.09)	*0.11(0.06)*	*0.09(0.04)*		*0.05*
Pd^4	0.16(0.12)	0.13(0.09)	0.07(0.03)		0.04
	0.14(0.09)	*0.11(0.06)*	*0.09(0.04)*		*0.05*
Pd^5	0.04(0.21)	−0.07(0.10)	−0.11(0.06)		−0.17
	0.05(0.25)	*−0.02(0.18)*	*−0.05(0.15)*		*−0.20*
N^1	−0.24(−0.24)	−0.18(−0.18)	−0.09(−0.09)	0.0	
	−0.25(−0.25)	*−0.24(−0.24)*	*−0.15(−0.15)*	*0.0*	
N^2	−0.13(−0.13)	−0.06(−0.06)	−0.09(−0.09)	0.0	
	−0.23(−0.23)	*−0.11(−0.11)*	*−0.15(−0.15)*	*0.0*	

[a] The values in the parentheses are the Mulliken atomic charges relative to the free N_2 and Pd_5 cluster fragment.

TABLE 4: Mulliken Bond Populations for the N−Pd in the Structures, 3NNa, 3NNb, and 3NNc Calculated at the B3LYP/I (plain) and B3LYP/III (italics) Levels

N−Pd	3NNa	3NNb	3NNc
N^1-Pd^5	0.108	0.096	0.016
	0.053	*0.041*	*0.002*
$N^1-Pd^{3,4}$	0.090	0.161	0.196
	0.087	*0.140*	*0.153*
$N^2-Pd^{1,2}$	0.200	0.209	0.196
	0.139	*0.156*	*0.153*

so that the MO is destabilized in energy and then the interaction is weakened, since the N^1 atom is geometrically rather shifted in the [1$\bar{1}$0] direction from the center of the rectangle made by the four Pd atoms in the first layer (see Figure 4). Thus, it is concluded that the molecular orientation and the tilted structure of the coordinated N_2 molecule are determined by the interaction of the lower N atom with the Pd atom in the second layer.

The nature of the bonding of N_2 with Pd in **3NNa**, **3NNb**, and **3NNc** discussed above is also supported by both Mulliken atomic charge and bond population analyses. On the basis of the atomic charges of the N and Pd atoms relative to the N atom of the free N_2 and the Pd atoms of the Pd_5 cluster fragment, one can find the electron flows from the Pd_5 cluster to the coordinated N_2 molecule (Table 3). In Table 3, the increase in the positive and negative charges for the Pd atoms and the N atoms, respectively, shows the electron back-donation from the occupied d orbitals of the Pd atoms to the unoccupied pπ* orbitals of the N atoms. One will readily know that the electron back-donation from the Pd^5 atom to the N_2 molecule is important especially in **3NNa**. The strength of the electron back-donation from the Pd^5 atom to the N_2 molecule would be reflected on the stability sequence, **3NNa** > **3NNb** > **3NNc**.

As shown in Table 4, in **3NNa**, the Mulliken bond population is the largest in the $N^2-Pd^{1,2}$ bonds. The population in the N^1-Pd^5 bond was as large as that in the $N^1-Pd^{3,4}$ bonds, which shows that the N^1 interacts with the Pd^5 in the second layer as well as the $Pd^{3,4}$ in the first layer. The sequence of the population in the N^1-Pd^5 bond, **3NNa** > **3NNb** > **3NNc**, is consistent with the results presented above.

NO. For NO, we also found the tilted structures, **3NOa** and **3NOb**, where the NO molecule is oriented in the [001] and [1$\bar{1}$0] direction, respectively. The $N-Pd^5$ distance is as short as the $N-Pd^{3,4}$ distances indicating the interaction of the N atom with the Pd^5 in the second layer in both **3NOa** and **3NOb**. The $O-Pd^{1,2}$ distances in **3NOa** are 0.5 Å longer than the corresponding $N^2-Pd^{1,2}$ distances in **3NNa** due to the electrostatic repulsion between the oxygen and the $Pd^{1,2}$ in the first layer. As a result, the tilt angle of 48.3° is larger than that for N_2, and is as large as that for CO although the electrostatic repulsion between the oxygen and Pd is smaller for NO than for CO (vide infra). The electron donation from the pπ* orbital of NO to the dσ+sp orbitals of the $Pd^{3,4}$ atoms in the local $NO-Pd^{3,4}$ system raises the NO molecule up (see section 3.2). It should be noted that the calculation at the B3LYP/I level without polarization function showed the different coordination feature. Since the repulsion between the oxygen and the $Pd^{1,2}$ is underestimated without polarization function, the local attractive interaction of NO with the $Pd^{2,5}$ and with the $Pd^{2,4}$ by the electron donation from the pπ* orbitals of NO to the dσ+sp orbitals of the Pd atoms as mentioned in the section 3.2 might cause the deviation from the structure with the C_s symmetry.

In **3NOb**, NO coordinates to the long-bridge site of $Pd^{3,4}$ by the end-on mode without a bend mentioned above, because the electron donation from the pπ* orbital of NO to the dσ+sp orbitals of the $Pd^{3,4}$ atoms having the long Pd−Pd distance is very weak. Therefore, the tilt angle is smaller than that in **3NOa**. The coordination structure largely deviates from the C_s symmetry even with the polarization function due to the strong electron donation from the pπ* orbitals of NO to the $Pd^{2,4}$ atoms and to the $Pd^{2,5}$ atoms having the short Pd−Pd distances. Although we did not find the significant difference in the coordination energy between **3NOa** and **3NOb**, **3NOb** is more stable by 3.5 kcal/mol than **3NOa** by this interaction.

CO. As well as NO, CO has the tilted structures, **3COa** and **3COb**, where CO is oriented in the [001] and [1$\bar{1}$0] directions, respectively. In **3COa**, the distances of $C-Pd^5$ and $C-Pd^{3,4}$ are 1.965 and 1.975 Å, respectively, indicating that the C atom interacts with the Pd atoms in both first and second layers. In contrast to NO, the CO molecule does not have an electron in the pπ* orbital to give the bent structure on the interaction with the $Pd^{3,4}$ by the end-on mode. However, the tilt angle is as large as that in **3NOa**, because the more polarized CO causes the stronger repulsion between the oxygen and the $Pd^{1,2}$ atoms. The orientation of the CO molecule also affects the tilt angle. Since the CO molecule is rather shifted to the bridge site of Pd^3-Pd^4 in **3COb** with the [1$\bar{1}$0] CO molecular orientation, the interaction of the C with the Pd^5 in the second layer through the electron back-donation from the dσ orbital of Pd^5 to the pπ* orbital of CO perpendicular to the Pd surface is weakened (vide supra), and then the large tilt angle of 66.3° is given. The sequence of the coordination energy, **3COa** > **3COb**, would be ascribed to the site preference of CO in the coordination by the end-on mode to the Pd atoms in the first layer, because CO would prefer the short-bridge site of $Pd^{3,4}$ in **3COa** rather than the long-bridge site of $Pd^{3,4}$ in **3COb** as shown in the section 3.2. As well as the Pd_1 and Pd_2 cluster systems, the Pd_5 cluster system showed the coordination energy sequence, CO > NO > N_2.

3.4. Pd_{25} System. We further extended the Pd_5 cluster of the 2Pd-layered (1 × 1) surface unit of Pd(110) to the Pd_{25} cluster consists of 12 Pd atoms of the (3 × 3) surface unit of Pd(110) in the first layer, nine Pd atoms in the second layer and four Pd atoms in the third layer to include the effects of surrounding Pd atoms, and examined the favorable coordination site and the coordination energy for the nonpolar N_2 and polar CO molecules.

N_2. Both tilted structures of N_2 oriented in the [001] and [1$\bar{1}$0] directions on the hollow site, which were found in the Pd_5 cluster system (section 3.3), did not exist even at the B3LYP level with

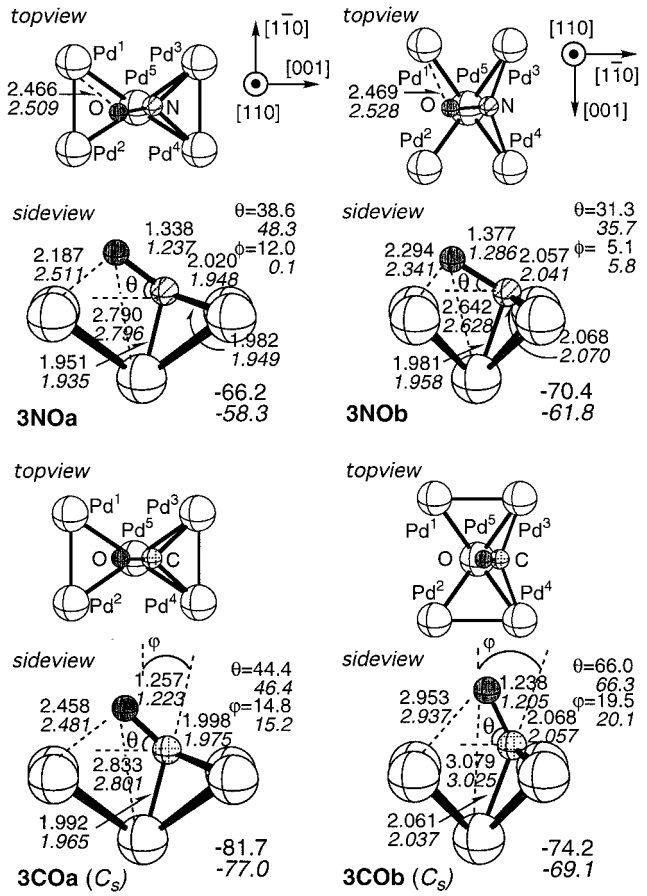

Figure 7. Optimized equilibrium structures of NO and CO molecules coordinated to the hollow site of Pd_5 cluster, the 2Pd-layered (1×1) surface unit of Pd(110), with the selected parameters (in Å and degrees) at the B3LYP/I (plain) and B3LYP/III (italics) levels, and their energies (in kcal/mol) relative to the Pd_5 cluster fragment and the free NO and CO molecules at those levels. The angles θ made by the NO- or CO-axis and the Pd surface, ϕ made by the NO-axis projected to the Pd surface and the [001] or [1$\bar{1}$0] axis and φ made by the Pd^5−C and [110] axes are presented. The symmetry of the structure **3NOa** was nearly C_s at the B3LYP/III level.

the basis set I for N_2 and the core part, the 2Pd-layered (1×1) surface unit, Pd_5, and the basis set VI for the other surrounding Pd atoms. The side-on and end-on structures of N_2 were found only on the bridge and top sites, respectively, as presented in Figure 8. The other N_2 bonded structures were not found because of the dissociation of N_2 from the Pd surface. The coordination energy of the end-on bonded N_2 on the top site, 7.4 kcal/mol, calculated at the B3LYP level was in excellent agreement with the experimentally observed one of 5.9 ± 1.4 kcal/mol for the upright-linear structure of N_2 on the top site.[9] The N_2 coordinations by the side-on mode to the long- and short-bridge sites were 15 kcal/mol endothermic.

To investigate the effects of the surrounding Pd atoms, we cut the part of Pd−N−N out from **4NNc** and performed the calculations for this Pd−N−N fragment. The negative charge on the N atom attached to the Pd atom in the Pd−N−N remarkably increased by the exclusion of the surrounding Pd atoms. This suggests that the σ-donation from the pσ orbital of N_2 to the dσ+sp orbital of the Pd atom decreased. In other words, this means that the σ-donation from the pσ orbital of N_2 to the dσ+sp orbital of Pd increased by the effect of the surrounding Pd atoms in the Pd_{25} system. This is because the coordination sites become electron deficient by the interaction with the surrounding Pd atoms, which enhances the electron

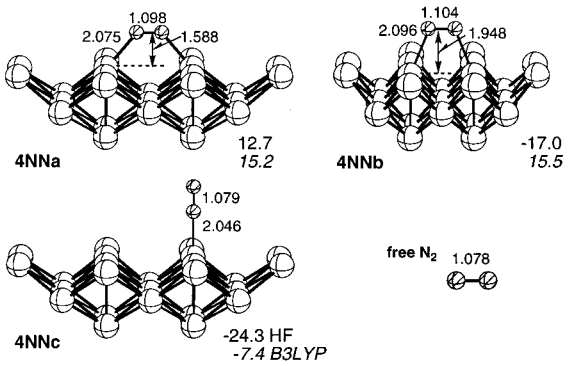

Figure 8. Optimized structures of N_2 molecule coordinated to the short- and long-bridge and top sites of the Pd_{25} cluster consists of 12 Pd atoms of the (3×3) surface unit of Pd(110) in the first layer, nine Pd atoms in the second layer, and four Pd atoms in the third layer, with the selected parameters (in Å) at the HF/VI level. In the optimizations, N_2 was forced to keep the canonical end-on or side-on coordination configuration. The energies (in kcal/mol) relative to the Pd_{25} cluster fragment and the free N_2 at the HF/VI (plain) and B3LYP/VI (italics) levels are also presented together.

TABLE 5: Gross Orbital Populations of the d Orbital of the Pd Atoms in the Pd Clusters, Pd_n ($n = 1, 2, 5, 25$), Calculated at the B3LYP/I, B3LYP/VI, and HF/VI Levels

cluster	site[a]	B3LYP/I	B3LYP/VI	HF/VI
Pd_1		10.000	10.000	10.000
long Pd_2		9.939	9.941	9.722
short Pd_2		9.812	9.887	9.896
Pd_5	Pd^{1-4}	9.523	9.819	9.823
	Pd^5	9.219	9.750	9.725
Pd_{25}	Pd^{1-4}		9.493	9.344
	Pd^5		9.471	9.116

[a] The sites in the core part which correspond to those in the Pd_5 cluster are presented for the Pd_{25} cluster.

donation from the pσ orbital of N_2 to the dσ+sp orbital of the Pd atom. To confirm the electron deficiency at the coordination sites in the Pd_{25} cluster, we calculated the gross orbital population of the d orbital of the Pd atoms and compared it among the Pd_n ($n = 1, 2, 5, 25$) clusters at the B3LYP/I, B3LYP/VI and HF/VI levels (Table 5).

In fact, the gross orbital population of the d orbital of the Pd atoms decreased with the increase in the number of Pd atom in the cluster model due to the incorporation of the unoccupied s and p orbitals in the interaction between the Pd atoms. On the other hand, it is obvious that the π-back-donation from the dπ orbitals of Pd to the pπ* orbitals of N_2 decreases by the electron deficiency at the coordination sites. Thus, the N_2 molecule prefers the end-on bonded structure on the top site where the σ-donation from the pσ orbital of the N_2 to the dσ+sp orbital of the Pd atom can dominantly contribute to the interaction of the N_2 with the Pd atom. The fact that the tilted structures of the N_2 on the hollow site and the N_2 end-on bonded structures on the bridge sites where the π-back-donation dominantly contributes to the interaction of the N_2 with the Pd atoms do not exist is therefore reasonably understood.

CO. Since we did not obtain any side-on bonded CO in the Pd_1, Pd_2, and Pd_5 cluster systems, only the end-on bonded structures were examined for CO in the Pd_{25} cluster system. The optimized coordination structures at the top, short- and long-bridge, and hollow sites and their coordination energies for CO are presented in Figure 9.

In contrast to the case of N_2, the tilted structure on the hollow site found in the Pd_5 cluster system also exists in the Pd_{25} system with only the [001] molecular orientation of CO (**4COe**). On

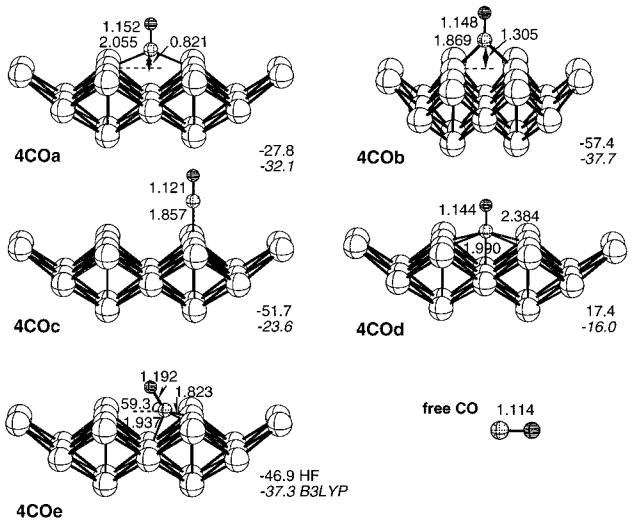

Figure 9. Optimized structures of CO molecule coordinated to the short- and long-bridge, top and hollow sites of the Pd_{25} cluster consists of 12 Pd atoms of the (3×3) surface unit of Pd(110) in the first layer, nine Pd atoms in the second layer, and four Pd atoms in the third layer, with the selected parameters (in Å and degrees) at the HF/VI level. In the optimizations, CO was forced to keep the canonical end-on coordination configuration except for **4COe** (C_s symmetry). The energies (in kcal/mol) relative to the Pd_{25} cluster fragment and the free CO at the HF/VI (plain) and B3LYP/VI (italics) levels are also presented together.

comparison among top, short- and long-bridge, and hollow sites, the short-bridge site was most favorable, which is in agreement with the results previously obtained by the density functional calculations with the basis set consisting of the plane waves.[11−13] The pseudolinear structure of CO with the tilt angle of 15° on the short-bridge site reported with the density functional calculations[11] was 0.2 kcal/mol less stable than the true linear structure in our calculations, which supports the previous interpretation[13] that the pseudolinear structure of CO comes from the repulsion between the polarized CO molecules aligned along the [1$\bar{1}$0] direction. The coordination energy of 37.7 kcal/mol was also in good agreement with the experimental result (35.7 kcal/mol).[26] The order of the preference of the coordination site was short-bridge (**4COb**) ≥ hollow (**4COe**) > long-bridge (**4COa**) > top (**4COc**) > hollow (**4COd**).

In the coordination of the strong π-acceptor molecule such as CO, the electron π-back-donation from the dπ orbitals of the Pd atoms to the CO pπ* orbitals as well as the electron donation from the CO pσ orbital to the dσ+sp orbitals of the Pd atoms is important even in the Pd_{25} cluster where the electron on the Pd atoms for the back-donation decreases. Therefore, the short-bridge site, where both electron σ-donation and π-back-donation most efficiently contribute to the interaction of CO with the Pd atoms, is preferred. The existence of the tilted structure on the hollow site, **4COe**, where the electron back-donation from the d orbitals of the Pd atoms to the CO pπ* orbitals is dominant in the interaction of CO with the Pd atoms, also originates from the strong π-acceptor character of CO.

4. Conclusions

The geometric and electronic structures of the N_2, NO, and CO molecules coordinated to the Pd clusters, Pd_n ($n = 1,2,5,-25$), as a model of Pd(110) surface were investigated by means of ab initio MO methods. The coordination structure of the N_2, NO, and CO molecules significantly depends on the nature of the interaction of these molecules with the Pd cluster and on the Pd cluster model. Only the end-on bonded structures were found in the Pd_1 system for all three molecules, N_2, NO, and CO. On the contrary, in the Pd_2 system, N_2 coordinates to the bridge site of Pd_2 clusters preferably by the side-on mode, although NO and CO prefer the end-on structure.

On the hollow site of the Pd_5 cluster, the 2 layered (1×1) surface unit of Pd(110), the tilted structures with an unconventional coordination mode were found for all three molecules. The coordination configuration largely deviates from the true end-on and side-on due to the strong interaction of the lower N or C atom with the Pd atom in the second layer through the electron back-donation from the occupied d orbital of the Pd atom to the unoccupied pπ* orbital of the admolecules. By the molecular orbital analysis, it was elucidated that the preferable [001] molecular orientation of the coordinated N_2 to the hollow site of the Pd_5 cluster is ascribed to the interaction of the lower N atom with the Pd atom in the second layer.

The tilted structures found in the Pd_5 cluster system for N_2 did not exist in the extended Pd_{25} cluster system, because the ability of the electron back-donation of Pd to the pπ* orbitals of N_2 is lowered while the electron donation from the N_2 pσ orbital to the Pd atoms remarkably increases. Therefore, the N_2 molecule favorably coordinates to the top site by the end-on mode in the Pd_{25} system by the interaction dominantly through the electron donation. On the other hand, the strong π-acceptor CO favorably coordinates to the short-bridge site by the end-on mode in the Pd_{25} system because the electron π-back-donation as well as the electron donation is important in the interaction of CO with the Pd atoms even in the Pd_{25} system. The tilted structure of CO on the hollow site, **4COe**, where the electron back-donation from the d orbitals of the Pd atoms to the pπ* orbitals of CO is dominant in the interaction of CO with the Pd atoms, also exists due to the strong π-acceptor character of CO.

Acknowledgment. The present study was supported by the Research and Development for Applying Advanced Computational Science and Technology of the Japan Science and Technology Corporation (Project ACT-JST-98-A5-1) and partially by a Grant-in-Aid for Scientific Research from the Ministry of Education, Science, Sports, and Culture in Japan. Numerical calculations were in part carried out at the Computer Center of the Institute for Molecular Science, Japan. M.N. thanks Professors S. Sakaki and Y. Matsumoto for their fruitful discussions and T.N. acknowledges a Postdoctoral Fellowship from the Project ACT-JST-98-A5-1.

References and Notes

(1) (a) Ozaki, A.; Aika, K. In *Catalysis: Science and Technology*; Anderson, J. R., Boudart, M., Eds.; Springer-Verlag KG: Berlin, 1981; Vol. 1, p 87. (b) *The Chemical Physics of Solid Surfaces and Heterogeneous Catalysis*; King, D. A.; Woodruff, D. P., Eds.; Elsevier: Amsterdam, 1982; Vol. 4. (c) Ertl, G. In *Catalysis: Science and Technology*; Anderson, J. R., Boudart, M., Eds.; Springer-Verlag KG: Berlin, 1983; Vol. 4, p 209.

(2) (a) Khan, M. M. T.; Martell, A. E. *Homogeneous Catalysis by Metal Complexes: Activation of Small Inorganic Molecules*; Academic Press: London, 1974; Vol. 1. (b) *New Trends in the Chemistry of Nitrogen Fixation*; Chatt, J., da Câmara Pina, G. L. M., Richards, R. L., Eds.; Academic Press: London, 1980.

(3) Sakaki, S.; Morokuma, K.; Ohkubo, K. *J. Am. Chem. Soc.* **1985**, *107*, 2686.

(4) Blomberg, M. R. A.; Siegbahn, P. E. M. *Chem. Phys. Lett.* **1991**, *179*, 524.

(5) (a) Mortensen, J. J.; Hammer, B.; Nørskov, J. K. *Phys. Rev. Lett.* **1998**, *80*, 4333. (b) Rod, T. H.; Hammer, B.; Nørskov, J. K. *Phys. Rev. Lett.* **1999**, *82*, 4054.

(6) For example, see; (a) Saillard, J.-Y.; Hoffmann, R. *J. Am. Chem. Soc.* **1984**, *106*, 2006. (b) Hay, P. J. *J. Am. Chem. Soc.* **1987**, *109*, 705.

(7) Grunze, M.; Driscoll, R. K.; Burland, G. N.; Cornish, J. C. L.; Pritchard, J. *Surf. Sci.* **1979**, *89*, 381.

(8) Grunze, M.; Golsze, M.; Hirschwald, W.; Freund, H.-J.; Pulm, H.; Seip, U.; Tsai, M. C.; Ertl, G.; Küppers, J. *Phys. Rev. Lett.* **1984**, *53*, 850.

(9) Kuwahara, K.; Jo, M.; Tsuda, H.; Onchi, M.; Nishijima, M. *Surf. Sci.* **1987**, *180*, 421.

(10) Grunze, M. In *The Chemical Physics of Solid Surfaces and Heterogeneous Catalysis*; King, D. A., Woodruff, D. P., Eds.; Elsevier: Amsterdam, 1982; Vol. 4, p 143.

(11) (a) Hu, P.; King, D. A.; Crampin, S.; Lee, M.-H.; Payne, M. C. *Chem. Phys. Lett.* **1994**, *230*, 501.

(12) Hu, P.; King, D. A.; Lee, M.-H.; Payne, M. C. *Chem. Phys. Lett.* **1995**, *246*, 73.

(13) Hu, P.; King, D. A.; Crampin, S.; Lee, M.-H.; Payne, M. C. *J. Chem. Phys.* **1997**, *107*, 8103.

(14) Frisch, M. J.; Trucks, G. W.; Schlegel, H. B.; Schlegel, G. E.; Robb, M. A.; Cheeseman, J. R.; Zakrzewski, V. G.; Montgomery, J. A., Jr.; Stratmann, R. E.; Burant, J. C.; Dapprich, S.; Millam, J. M.; Daniels, A. D.; Kudin, K. N.; Strain, M. C.; Farkas, O.; Tomasi, J.; Barone, V.; Cossi, M.; Cammi, R.; Mennucci, B.; Pomelli, C.; Adamo, C.; Clifford, S.; Ochterski, J.; Petersson, G. A.; Ayala, P. Y.; Cui, Q.; Morokuma, K.; Malick, D. K.; Rabuck, A. D.; Raghavachari, K.; Foresman, J. B.; Cioslowski, J.; Ortiz, J. V.; Stefanov, B. B.; Liu, G.; Liashenko, A.; Piskorz, P.; Komaromi, I.; Gomperts, R.; Martin, R. L.; Fox, D. J.; Keith, T.; Al-Laham, M. A.; Peng, C. Y.; Nanayakkara, A.; Gonzalez, C.; Challacombe, M.; Gill, P. M. W.; Johnson, B.; Chen, W.; Wong, M. W.; Andres, J. L.; Gonzalez, C.; Head-Gordon, M.; Replogle, E. S.; Pople, J. A. *Gaussian 98*, revision A.3; Gaussian, Inc.: Pittsburgh, PA, 1998.

(15) Becke, A. D.; *J. Chem. Phys.* **1993**, *98*, 5648.

(16) Hay, P. J.; Wadt, W. R. *J. Chem. Phys.* **1985**, *82*, 299.

(17) Hariharan, P. C.; Pople, J. A. *Theor. Chim. Acta* **1973**, *28*, 213.

(18) Ehlers, A. W.; Böhme, M.; Dapprich, S.; Gobbi, A.; Höllwarth, A.; Jonas, V.; Köhler, K. F.; Stegmann, R.; Veldkamp, A.; Frenking, G. *Chem. Phys. Lett.* **1993**, *208*, 111.

(19) Scott, A. P.; Radom, L. *J. Phys. Chem.* **1996**, *100*, 16502.

(20) Hay, P. J.; Wadt, W. R. *J. Chem. Phys.* **1985**, *82*, 270.

(21) Rao, C. N.; Rao, K. K. *Can. J. Phys.* **1964**, *42*, 1336.

(22) The calculated N−N vibrational frequency of the free N_2, 2458 cm^{-1}, at the B3LYP/III level was in very good agreement with the experimentally observed one, 2331 cm^{-1}(see: Whitman, L. J.; Bartosch, C. E.; Ho, W.; Strasser, G.; Grunze, M. *Phys. Rev. Lett.* **1986**, *56*, 1984.)

(23) Noell, J. O.; Morokuma, K. *Inorg. Chem.* **1979**, *18*, 2774.

(24) CO is more polarized than NO as shown in the Mulliken atomic charges; N(+0.115 e)−O(−0.115 e), C(+0.157 e)−O(−0.157 e).

(25) The couples of (bonding MO: antibonding MO) are as follows; **3NNa**: (28a′:59a′), (35a″:80a″), (36a′:61a′), (40a″:71a″), (51a″:72a″); **3NNb**: (30a′:60a′), (40a″:88a″), (44a″:69a″), (49a′:58a′), (52a″:78a″).

(26) Raval, R.; Haq, S.; Harrison, M. A.; Blyholder, G.; King, D. A. *Chem. Phys. Lett.* **1990**, *167*, 391.